[Research Paper] 대한금속 · 재료학회지 (*Korean J. Met. Mater.*), Vol. 62, No. 4 (2024) pp.284-291
DOI: 10.3365/KJMM.2024.62.4.284

Surfactant Composition Dependent Evolution of Electronic/Structural Properties of P3HT Nanoparticle Colloids Synthesized via Mini-Emulsion Technique

Byoung-Nam Park*

Department of Materials Science and Engineering Hongik University 72-1, Sangsu-dong, Mapo-gu, Seoul 04066, Republic of Korea.

Abstract: This study investigates the influence of surfactant (sodium dodecyl sulfate, SDS) concentration on the size and optoelectronic properties of poly(3-hexylthiophene) (P3HT) nanoparticles (NPs) synthesized via the mini-emulsion technique. P3HT NPs were fabricated with varying SDS concentrations. The size dependent optoelectronic properties, including the highest occupied molecular orbital (HOMO) and the lowest unoccupied molecular orbital (LUMO) levels, were analyzed through photoelectron spectroscopy in air, UV-Vis absorption spectroscopy and cyclic voltammetry. A clear trend of decreasing NP size with increasing SDS concentration was observed. Higher SDS levels resulted in smaller NPs with enhanced pi-pi stacking and shorter conjugation lengths. This structural change led to a noticeable shift in HOMO and LUMO levels, indicating a direct correlation between surfactant concentration and the electronic properties of the P3HT NPs. The absorption spectra revealed a decrease in the A0-0/A0-1 ratio with smaller NP size, suggesting a transition towards more pronounced H-aggregate characteristics. As the size of the P3HT NPs decreases, there is a notable increase in H-aggregate formation. This increase can be attributed to enhanced interchain interactions between the polymer chains. In smaller NPs, the surface area-to-volume ratio is higher, leading to more significant interactions between adjacent polymer chains. These interactions promote the formation of H-aggregates, characterized by their interchain pi-pi stacking, which differs from the intrachain coupling observed in J-aggregates.

(Received 30 November, 2023; Accepted 22 December, 2023)

Keywords: P3HT colloids, mini-emulsion, aggregates, surfactant, conjugation

1. INTRODUCTION

The dynamic field of organic electronics, marked by rapid advances and growing applications, is undergoing a paradigm shift with the emergence of polymer-based nanomaterials[1-3]. Among these, poly(3-hexylthiophene) (P3HT), a semiconducting polymer, has been the subject of extensive research due to its promising applications in organic solar cells, field-effect transistors, and organic light-emitting diodes[4-7]. The allure of P3HT stems from its favorable electronic properties, ease of processing, and the potential for tunable optoelectronic characteristics.

In this study the mini-emulsion technique, noted for its ability to control particle size and distribution, crucial determinants of the material's electronic properties, was employed to synthesize P3HT nanoparticles (NPs).[8-10] This method, characterized by its use of surfactants to stabilize the emulsion, ensures the formation of NPs with defined dimensions and morphologies, directly influencing the conjugation length and intermolecular interactions within the polymer.

In this realm, the choice of surfactant is not merely a procedural necessity but a strategic tool that can be used to manipulate the NP properties. Here, we specifically focus on sodium dodecyl sulfate (SDS) due to its compatibility with P3HT, its cost-effectiveness, and the ability to form stable emulsions. The concentration of SDS was hypothesized to play a pivotal role in determining the size of the P3HT NPs. This size factor, in turn, has profound implications on the optoelectronic properties of the polymer, as it influences the

- 박병남: 교수
*Corresponding Author: Byoung-Nam Park
[Tel: +82-10-4244-0495, E-mail: metalpbn@gmail.com]

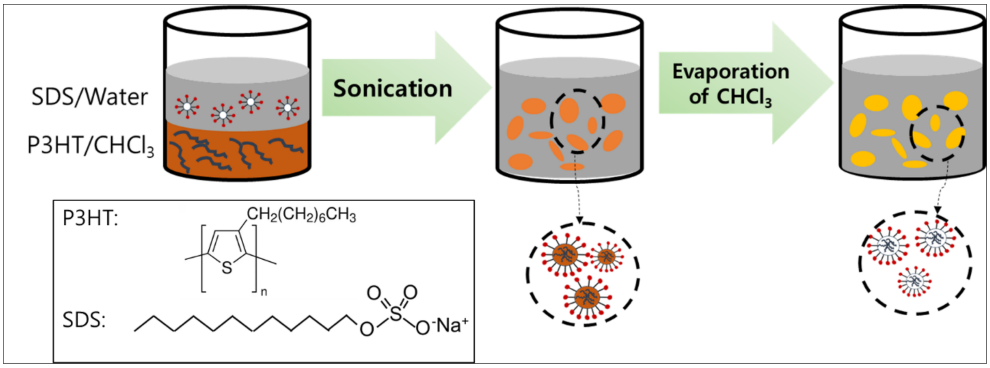

Fig. 1. Schematics of the mini-emulsion process to produce P3HT colloids

extent of pi-pi stacking and conjugation length within the polymer chains.

The electronic structure of conjugated polymers like P3HT is inherently linked to their physical dimensions and morphological characteristics. The highest occupied molecular orbital (HOMO) and the lowest unoccupied molecular orbital (LUMO) levels, key parameters defining the electronic behavior of these materials, are sensitive to changes in molecular ordering and interchain interactions[11-14]. Consequently, controlling the NP size through surfactant concentration provides a way of fine-tuning these energy levels, thereby tailoring the material's absorption, emission, and charge transport properties.

Beyond size control, this study also investigated the structural properties of the P3HT NPs, particularly focusing on the conjugation length and pi-pi stacking. These features are integral to the optoelectronic performance of the polymer. The conjugation length affects the effective bandgap, influencing light absorption and emission characteristics, while pi-pi stacking is crucial for charge mobility, a key factor in device efficiency.

This paper aims to elucidate the relationship between surfactant composition, specifically SDS concentration, and the resultant size and structural properties of P3HT NPs synthesized via the mini-emulsion technique. Through a systematic study combining NP characterization, including their electrochemical and optoelectronic properties, with electronic property analysis, we seek to provide deeper insights into how surfactant-induced changes at the nanoscale can be leveraged to optimize the optoelectronic behavior of P3HT. Here, we investigated P3HT colloid size dependent optoelectronic properties, including the HOMO and the LUMO levels, using photoelectron spectroscopy in air, UV-Vis absorption spectroscopy and cyclic voltammetry measurements. This research not only contributes to the fundamental understanding of polymer NP synthesis but also has significant implications for the design and development of next-generation organic electronic devices.

2. MATERIALS AND METHODS

2.1. Mini-Emulsion Technique for P3HT Colloid Formation

High-regioregularity poly(3-hexylthiophene) (P3HT), characterized by a regioregularity exceeding 96%, was acquired from Sigma-Aldrich. Complementary materials, including sodium dodecylbenzene sulfonate (SDS) and anhydrous chloroform, were also sourced from Sigma-Aldrich. We utilized the mini-emulsion technique for the synthesis of P3HT colloids. The process began by dissolving 10.0 mg of P3HT in 1 mL of chloroform. This mixture was stirred continuously for 12 hours at a stable temperature of 45°C, resulting in a 10 mg/mL P3HT solution with an estimated thickness of 60 nm. Subsequently, this P3HT solution was mixed with pre-prepared SDS aqueous solutions of varying concentrations (1.0, 1.7, 3.4, and 10 mM). Following sonication for 5 minutes, the mixture was heated at 70°C for one hour to ensure complete chloroform evaporation. This process ultimately yielded an aqueous suspension of P3HT colloids. A comprehensive schematic of the mini-emulsion technique, delineating the synthesis stages, is illustrated in Figure 1.

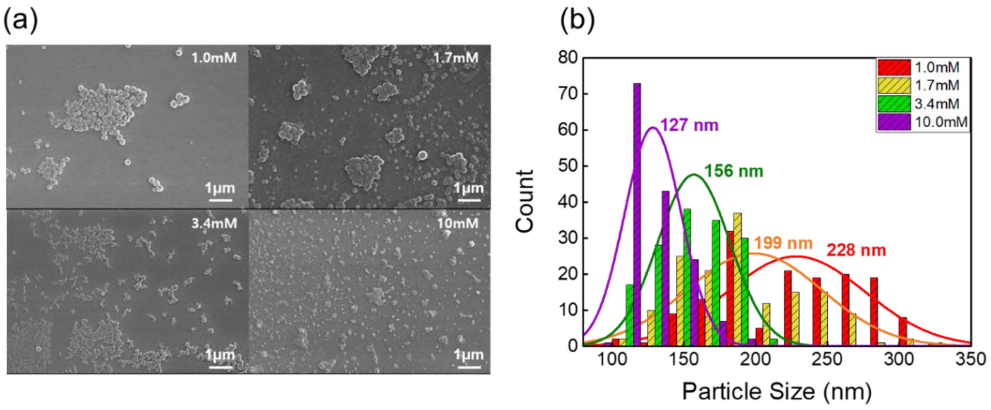

Fig. 2. (a) SEM images of P3HT colloids synthesized with different SDS concentrations (b) SDS concentration dependent size distribution of P3HT colloids

2.2. Structural and Optoelectronic/Electrochemical Characterizations of P3HT Colloids

For morphological analysis, we first coated silicon substrates with a thin layer of P3HT colloids, followed by air-drying at 70°C. The structural features of these colloids were then examined using a scanning electron microscope (SEM), as illustrated in Figure 2(a).

SEM analysis was carried out post-sample preparation, which involved drop-casting the P3HT colloids onto silicon substrates and subsequently drying them at 70°C. To explore the impact of SDS concentration on P3HT nanoparticle size, we performed SEM image analysis. This analysis revealed size distributions that varied with SDS concentration, as shown in Figure 2(b).

To study size dependent structural properties, optical absorption spectroscopic methods were used with a photo-spectrometer after coating P3HT colloids on glass substrates. The size dependent ionization energy of P3HT NPs was measured using photoelectron spectroscopy in air (PESA). CV measurements were conducted to determine the LUMOs and HOMOs of P3HT NPs.

The redox potentials were measured in a solution of 0.1 M tetrabutylammonium perchlorate (TBAP) in acetonitrile (ACN), using platinum electrodes for both the working and counter electrodes at a scan rate of 10 mV/s. The measurements were referenced against an Ag/AgCl electrode. The ferrocenium/ferrocene (Fc^+/Fc) couple exhibited an oxidation potential of +0.51 V and a reduction potential of +0.43 V, both values being relative to the Ag/AgCl reference electrode. The HOMO levels were calculated by HOMO (eV)=e(-4.8 V-(E_{onset}=$E_{1/2}$(Fc^+/Fc))[15].

2.3. Electrical Characterization Using Field Effect Transistor Devices

We fabricated a bottom-contact field-effect transistor (FET) to investigate charge transport in the P3HT colloid films near the SiO_2 interface. The source and drain electrodes, composed of Au (80 nm) over Ti (3 nm), were patterned on a 200 nm SiO_2 gate dielectric via photolithography. A highly-doped silicon substrate served as the gate electrode. The P3HT NP colloids were then drop-casted onto this pre-patterned substrate and subsequently heated at 80°C to evaporate water. For the FET measurements, we covered the P3HT channel region with glass. Electrical characterizations of the FET were conducted in air using a semiconductor parameter analyzer (HP4145B).

3. RESULTS AND DISCUSSION

The relationship between the size of the synthesized P3HT NPs and the concentration of SDS is illustrated in Figure 2. Figure 2(a) shows SEM images of the P3HT NP colloids synthesized with different concentrations of SDS. Figure 2(b) offers a detailed analysis of the size distribution of these nanoparticles, showcasing how changes in SDS concentration affected NP size. Notably, the size distribution of P3HT NPs varied with different concentrations of SDS. A clear trend was observed, where an increase in SDS

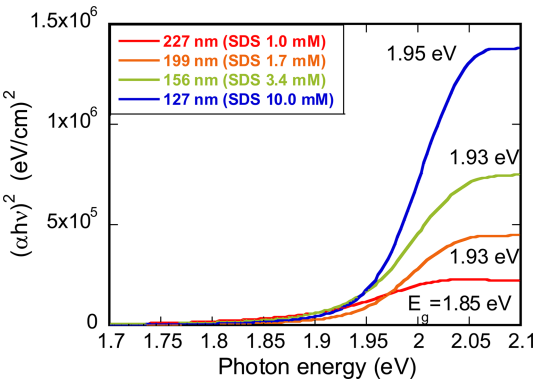

Fig. 3. Tauc plots for different sizes of P3HT colloids

concentration resulted in a corresponding decrease in the size of the NPs.

The observed dependence of P3HT NP size on the concentration of SDS in the mini-emulsion synthesis process, specifically the trend of decreasing NP size with increasing SDS concentration, can be explained by several key factors in colloidal chemistry and NP formation. SDS, being a surfactant, forms micelles in aqueous solutions above its critical micelle concentration. As the concentration of SDS increases, the number of micelles in the solution also increases. These micelles act as templates or nano-reactors for the formation of nanoparticles. With more micelles present at higher SDS concentrations, the P3HT is distributed among a greater number of micelles, leading to the formation of smaller NPs. At higher concentrations, more SDS molecules are available to stabilize the NPs, effectively preventing them from aggregating or growing too large. This stabilization is critical to the final size of the NPs. The process of NP formation involves nucleation followed by growth. Higher SDS concentrations can lead to a higher nucleation rate due to the increased number of micelles. This results in a larger number of smaller nuclei, which eventually grow into smaller NPs. Conversely, at lower SDS concentrations, fewer nuclei form, which can grow larger due to the availability of more P3HT per nucleus.

The energy band gap of the P3HT NPs was determined using the Tauc plot derived from optical absorption data presented in Figure 3. We observed that as the size of the P3HT NP decreased from 227 nm to 127 nm, the energy band gap correspondingly increased, moving from 1.85 eV to 1.95 eV, respectively.

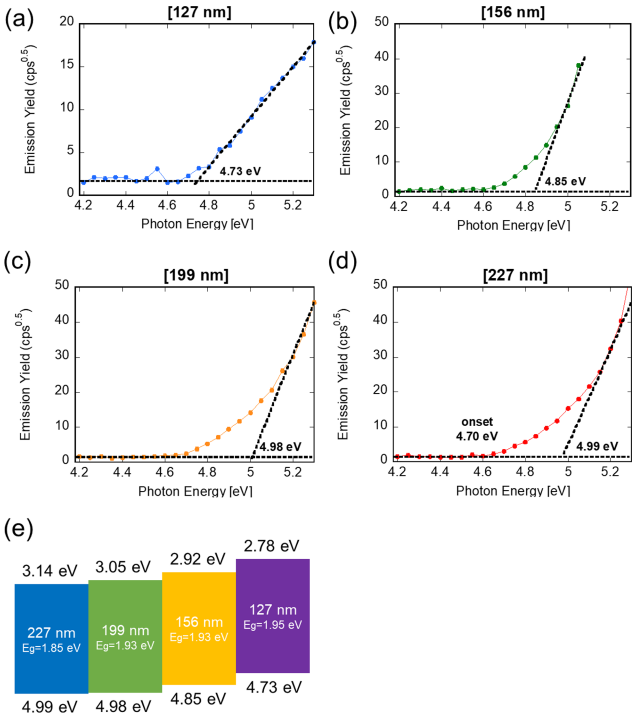

Fig. 4. Plots of the emission yield as a function of photon energy for (a) 127 nm (b) 156 nm (c) 199 nm (d) 227 nm P3HT colloids. (e) Energy band diagrams representing the LUMO, HOMO energy levels, and energy band gap (Eg) of P3HT colloids of different sizes.

Using the PESA analysis, the ionization energy of P3HT NPs with different sizes was measured, as shown in Figure 4. PESA is a technique used to measure the ionization potential of materials, and is particularly useful for the analysis of thin films and surfaces[16]. Unlike vacuum-based photoelectron spectroscopy methods, PESA allows measurements to be conducted in an ambient air environment, which can be advantageous for studying materials sensitive to vacuum conditions, or those that require a rapid analysis. In PESA, the sample is irradiated with photons of varying energies from 4.2 to 5.3 eV. As the photon energy increases, electrons are emitted from the sample surface. The number of emitted electrons (emission yield) is measured and plotted against the photon energy. We measured the ionization potential by identifying the threshold energy at which electrons start to be emitted from the sample. This threshold corresponds to the minimum photon energy required to overcome the binding energy of the outermost electrons in the material. Initially, at lower photon energies, no electrons are emitted, and the emission yield is zero. As the photon energy reaches the

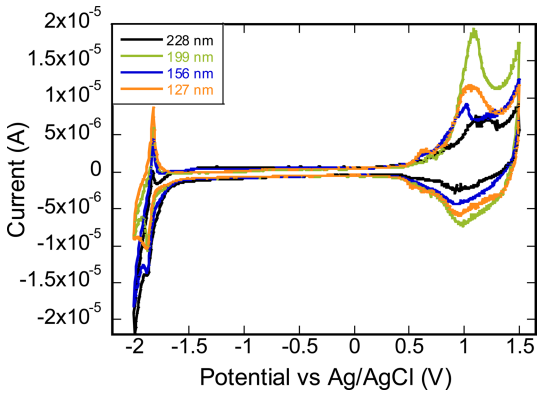

Fig. 5. CV plots for P3HT colloids of different sizes

ionization threshold, electrons begin to be emitted, and the emission yield increases sharply. The plot is analyzed by looking for the point where the emission yield graph intersects the photon energy axis. This intersection point is indicative of the threshold energy.

Utilizing data from PESA and optical absorption studies, we determined the LUMO and HOMO levels of P3HT NPs of varying sizes. An increase in NP size was found to correspond with a rise in ionization potential, as depicted in Figure 4(e). Smaller NPs have a larger surface-to-volume ratio, which can influence their electronic properties due to surface states. These surface states can alter the energy levels of the electronic states of the NPs. As the NP size increases, the influence of surface states diminishes, potentially leading to a higher ionization potential.

CV measurements were conducted to verify the size-dependent energy levels of P3HT NP colloids in Figure 5. The HOMO and LUMO levels of a material can be estimated from CV measurements by analyzing the onset of oxidation and reduction processes. The onset of the oxidation peak corresponds to the removal of an electron from the HOMO level. This is where the material starts to oxidize. The potential at this onset can be related to the HOMO energy level relative to the reference electrode.

Table 1. Summary of LUMOs, HOMOs, and energy band gap for P3HT colloids of different sizes.

P3HT NP size	HOMO (eV)	LUMO (eV)	Band Gap (eV)
229 nm	-5.13	-2.67	2.46
199 nm	-5.16	-2.57	2.59
156 nm	-4.94	-2.57	2.37
127 nm	-5.08	-2.56	2.52

Similarly, the onset of the reduction peak corresponds to the addition of an electron to the LUMO level. This is where the material starts to reduce. The potential at this onset gives information about the LUMO energy level. The potentials obtained for the HOMO and LUMO levels are referenced to the Fermi level of the standard electrode.

Table 1 summarizes the general trend of band gap variation with the size of P3HT NPs. Notably, there's an observed decrease in the band gap as the NP size increases from 127 nm to 229 nm. However, the 199 nm P3HT NPs deviate from this trend. This anomaly could potentially be explained by polydispersity within the NP samples. If the 199 nm batch exhibits a broader size distribution, it would influence the averaged energy levels obtained from CV measurements, possibly accounting for the unexpected increase in the band gap.

Size dependent aggregate structural information was extracted from the absorption spectra. The peaks around 550 nm and 600 nm in Figure 6(a) were assigned as A_{0-1} and A_{0-0},

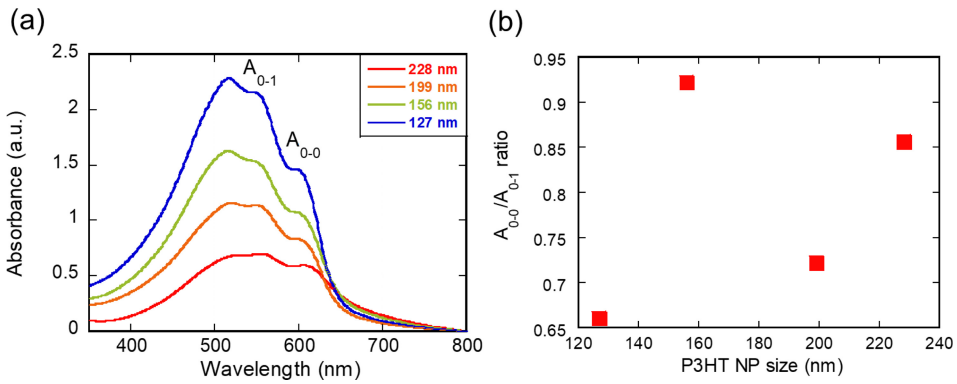

Fig. 6. (a) Optical absorption and (b) ratio of A0-0 toA0-1 for P3HT colloids of different sizes.

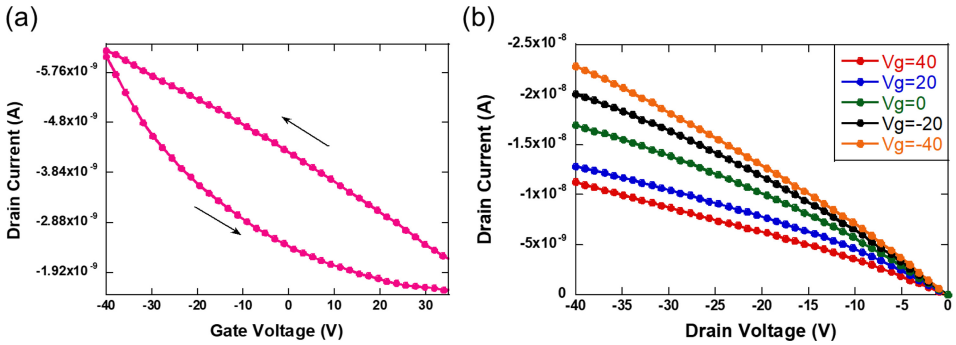

Fig. 7. (a) ID-VG and (b) ID-VD characteristic curves for P3HT NP colloids (227 nm)

respectively. The $A_{0\text{-}0}/A_{0\text{-}1}$ ratio in the absorption spectrum is a crucial indicator for distinguishing between H-aggregates and J-aggregates in conjugated polymers like P3HT[17,18]. In J-aggregates, the chromophores are aligned in such a way that their transition dipoles are coherently additive. This leads to a sharp, intense 0-0 (first electronic transition) peak and a weaker 0-1 peak. As a result, J-aggregates typically exhibit a high $A_{0\text{-}0}/A_{0\text{-}1}$ ratio. J-aggregates are indicative of strong intrachain interactions and extended conjugation.

For H-aggregates, the chromophores are aligned in a manner that causes their transition dipoles to more or less cancel each other out. This alignment typically results in a less intense or even absent 0-0 peak and a more pronounced 0-1 peak. Therefore, H-aggregates show a low $A_{0\text{-}0}/A_{0\text{-}1}$ ratio. H-aggregates are characteristic of strong interchain interactions and possibly shorter conjugation lengths. So, if the $A_{0\text{-}0}/A_{0\text{-}1}$ ratio decreases, it suggests a transition from J-aggregate dominance to H-aggregate dominance. This shift indicates an increase in interchain interactions relative to intrachain interactions, which can significantly affect the material's optical and electronic properties.

Figure 6(b) displays the $A_{0\text{-}0}/A_{0\text{-}1}$ ratios for all P3HT NP samples, which were found to be less than 1. This suggests a predominance of H-type aggregation, indicative of robust interchain interactions[19]. As the size of the P3HT NPs diminished, there was a corresponding decrease in the $A_{0\text{-}0}/A_{0\text{-}1}$ ratio, underscoring stronger H-aggregate formation. The exception was observed in the 156 nm sample, where the $A_{0\text{-}0}/A_{0\text{-}1}$ ratio did not follow the general trend, potentially due to a broad size distribution within the sample. The decrease in the $A_{0\text{-}0}/A_{0\text{-}1}$ ratio in the absorption spectrum of P3HT NPs with decreasing size, especially when synthesized via the mini-emulsion technique, can be attributed to changes in the molecular and aggregate structure within the NPs.

As the size of P3HT NPs decreases, there's a likelihood of increased pi-pi stacking between polymer chains (interchain coupling). This interchain coupling is characteristic of H-aggregates, which typically show a lower $A_{0\text{-}0}/A_{0\text{-}1}$ ratio. The smaller the NPs, the greater the surface area relative to volume, which could enhance interactions between polymer chains, leading to more pronounced H-aggregate formation. Further, in smaller NPs, the confined space may force polymer chains into closer proximity, favoring interchain interactions over intrachain interactions. J-aggregates, which are indicative of strong intrachain interactions and show a higher $A_{0\text{-}0}/A_{0\text{-}1}$ ratio, might be less favored in these confined environments.

The electrical characteristics of P3HT NPs were investigated using field-effect transistors (FETs). Transfer characteristic curves indicated that P3HT NPs constitute *p*-channel FETs, with the gate voltage magnitude inversely related to the drain voltage. However, output transistor curves did not exhibit clear current saturation. This absence of saturation could stem from several factors. Notably, high contact resistance at the source/drain interfaces might obscure the pinch-off phenomenon due to dense packing of P3HT NPs near these contacts[20]. This, in turn, can cause a significant voltage drop at the contacts, which may lead to misinterpretation of the channel's actual voltage. Furthermore, undetectable current at low drain voltage could imply insufficient drive voltage for carrier injection or high resistance pathways. Additionally, traps and defects within

the P3HT semiconductor can hinder carrier mobility and alter recombination dynamics, potentially resulting in atypical *I-V* characteristics that deviate from the expected pinch-off behavior[21,22].

4. SUMMARY AND CONCLUSIONS

In this study, we investigated the correlation between the size of P3HT NPs and their aggregate formation and electronic properties. Our findings demonstrate a clear relationship between the nanoparticle size and the type of chromophore aggregation, as well as the energy band gap of the material.

As the size of P3HT NPs decreases, there is a notable increase in H-aggregate formation. This increase can be attributed to enhanced interchain interactions between the polymer chains. In smaller NPs, the surface area-to-volume ratio is higher, leading to more significant interactions between adjacent polymer chains. These interactions promote the formation of H-aggregates, characterized by their interchain pi-pi stacking, which differs from the intrachain coupling observed in J-aggregates.

Concurrently, a decrease in P3HT NP size results in an increase in the energy band gap. This phenomenon is likely linked to the enhanced formation of H-aggregates and the associated changes in electronic structure. As the NPs become smaller, the altered molecular packing and increased interchain interactions lead to a reduction in the conjugation length and an increase in the band gap. This shift in the band gap is indicative of changes in the electronic and optical properties of the P3HT material, which are crucial for applications in organic electronics and photovoltaics.

In conclusion, the size of the P3HT NPs plays a critical role in determining their aggregate structure and electronic properties. The observed increase in H-aggregate formation and the corresponding rise in the energy band gap with decreasing nanoparticle size provide valuable insights for tailoring the material properties of P3HT for specific applications in nanotechnology and materials science. Understanding these relationships is essential for the development and optimization of organic electronic devices, where the control of material properties at the nanoscale can significantly impact performance and efficiency.

ACKNOWLEDGEMENT

This research was supported by the Basic Science Research Program through the National Research Foundation of Korea (NRF) funded by the Ministry of Education (NRF-2015R1A6A1A03031833, NRF-2019R1F1A1060042 and NRF-2020R1A2C1007258). This work was also supported by the 2024 Hongik Faculty Research Support Fund.

REFERENCES

1. Fahlman, M. Fabiano, S. Gueskine, V. Simon, D. Berggren, M. Crispin, X., *Nature Reviews Materials* **4**, 627 (2019).
2. Bronstein, H. Nielsen, C. B. Schroeder, B. C. McCulloch, I., *Nature Reviews Chemistry* **4**, 66 (2020).
3. Friederich, P. Fediai, A. Kaiser, S. Konrad, M. Jung, N. Wenzel, W., *Advanced Materials* **31**, 1808256 (2019).
4. R. Murad, A. Iraqi, A. Aziz, S. B. N. Abdullah, S. Brza, M. A., *Polymers* **12**, 2627 (2020).
5. Ates, M. Karazehir, T. Sezai Sarac, A., *Current Physical Chemistry* **2**, 224 (2012).
6. Patil, A. Heeger, A. Wudl, F., *Chemical Reviews* **88**, 183 (1988).
7. Kim, Y. Ko, H. Park, B., *Materials Chemistry and Physics* **223**, 576 (2019).
8. Darwis, D., *Natural Science: Journal of Science and Technology* **9**, 4 (2020).
9. Pan, H. Tan, B. Yazdani, A. Budhlall, B. Sobkowicz, M. J., *Colloids and Surfaces A: Physicochemical and Engineering Aspects* **594**, 124633 (2020).
10. Tan, B. Li, Y. Palacios, M. F. Therrien, J. Sobkowicz, M. J., *Colloids and Surfaces A: Physicochemical and Engineering Aspects* **488**, 7 (2016).
11. Khlaifia, D. Ewels, C. P. Massuyeau, F. Chemek, M. Faulques, E. Duvail, J.-L. Alimi, K., *RSC Advances* **6**, 56174 (2016).
12. Guo, Z. Lee, D. Schaller, R. D. Zuo, X. Lee, B. Luo, T. Gao, H. Huang, L., *Journal of the American Chemical Society* **136**, 10024 (2014).
13. Yamagata, H. Spano, F. C., *The Journal of Chemical Physics* **136,** 184901 (2012).
14. Kim, Y. Park, B. N., *Applied Sciences* **10**, 6886 (2020).
15. Acevedo-Peña, P. Baray-Calderón, A. Hu, H. González, I. Ugalde-Saldivar, V. M., *Journal of Solid State Electrochemistry* **21**, 2407 (2017).
16. Yoshino, K. Onoda, M. Manda, Y. Yokoyama, M.,

Japanese Journal of Applied Physics **27**, L1606 (1988).
17. Spano, F. C. Silva, C., *Annual Review of Physical Chemistry* **65**, 477 (2014).
18. Ziffer, M. E. Jo, S. B. Liu, Y. Zhong, H. Mohammed, J. C. Harrison, J. S. Jen, A. K.-Y. Ginger, D. S., *The Journal of Physical Chemistry C* **122**, 18860 (2018).
19. Eder, T. Stangl, T. Gmelch, M. Remmerssen, K. Laux, D. Höger, S. Lupton, J. M. Vogelsang, J., *Nature Communications* **8**, 1641 (2017).
20. Waldrip, M. Jurchescu, O. D. Gundlach, D. J. Bittle, E. G., *Advanced Functional Materials* **30**, 1904576 (2020).
21. Un, H. I. Cheng, P. Lei, T. Yang, C. Y. Wang, J. Y. Pei, J., *Advanced Materials* **30**, 1800017 (2018).
22. Koehler, M. Biaggio, I., *Physical Review B* **70**, 045314 (2004).